The Journal of Immunology

IL-23–Mediated Psoriasis-Like Epidermal Hyperplasia Is Dependent on IL-17A

Heather L. Rizzo, Shinji Kagami, Kevin G. Phillips, Stephen E. Kurtz, Steven L. Jacques and Andrew Blauvelt

J Immunol 2011; 186:1495-1502; Prepublished online 20 December 2010;
doi: 10.4049/jimmunol.1001001
http://www.jimmunol.org/content/186/3/1495

Supplementary Material **http://www.jimmunol.org/content/suppl/2010/12/22/jimmunol.1001001.DC1**

References This article **cites 34 articles**, 7 of which you can access for free at:
http://www.jimmunol.org/content/186/3/1495.full#ref-list-1

The Journal of Immunology is published twice each month by
The American Association of Immunologists, Inc.,
1451 Rockville Pike, Suite 650, Rockville, MD 20852

Print ISSN: 0022-1767 Online ISSN: 1550-6606.

IL-23–Mediated Psoriasis-Like Epidermal Hyperplasia Is Dependent on IL-17A

Heather L. Rizzo,*,[1] Shinji Kagami,*,[1] Kevin G. Phillips,*,† Stephen E. Kurtz,‡ Steven L. Jacques,*,† and Andrew Blauvelt*,‡,§

IL-23 and Th17 cells producing IL-17A and IL-22 are found in excess in skin affected by psoriasis. Previous studies showed that IL-22, but not IL-17A, mediates psoriasis-like epidermal hyperplasia following recombinant murine (rm)IL-23 injections into skin. To further investigate the role of IL-17A, ears of mice were injected with rmIL-23. Investigators blinded to treatment conditions and mouse genotypes measured ear swelling, epidermal thickness, and cytokine expression. In wild-type (WT) mice, rmIL-23 induced ear swelling ($p < 0.001$, all p values versus saline), epidermal hyperplasia by histology ($p < 0.001$) and confocal microscopy ($p < 0.004$), and expression of both IL-17A and IL-22. As expected, rmIL-23 injections into *IL-22*$^{-/-}$ mice resulted in relatively little ear swelling ($p < 0.09$) and epidermal hyperplasia ($p < 0.51$ by histology and $p < 0.75$ by confocal microscopy). Notably, rmIL-23 injections into *IL-17A*$^{-/-}$ mice produced little ear swelling ($p < 0.001$, versus IL-23–injected WT mice) and epidermal hyperplasia ($p < 0.001$ by histology and $p < 0.005$ by confocal microscopy), even though IL-22 was readily induced in these mice. Furthermore, systemic delivery of blocking Abs directed against either IL-22 or IL-17A completely inhibited IL-23–induced epidermal hyperplasia in WT mice. These results demonstrate that IL-17A, like IL-22, is a downstream mediator for IL-23–induced changes in murine skin and that both of these Th17 cytokines are necessary to produce IL-23–mediated skin pathology. IL-17A may represent an attractive therapeutic target in individuals with psoriasis by blocking downstream effects of IL-23. ***The Journal of Immunology*****, 2011, 186: 1495–1502.**

Cytokines produced by T cells are predominant mediators of skin pathology in psoriasis, a chronic inflammatory skin disease. Accumulating evidence suggests that IL-23 and the subsequent Th17 cell response it promotes are central factors in the pathogenesis of this disease (1). In psoriatic lesions, mRNAs for both IL-23 subunits (*IL-23p19* and *IL-12/23p40*) are elevated (2–4) and numerous IL-23^{+} dendritic cells are present (2, 5–7). Messenger RNAs for Th17 cytokines and chemokines (*IL-17A*, *IL-17F*, *IL-21*, *IL-22*, *TNF-α*, and *CCL20*) along with Th17 cells are increased (4, 8–13). Psoriatics also have high circulating levels of Th17 cells and cytokines (14). In addition, specific polymorphisms in *IL-23p19*, *IL-12/23p40*, and *IL-23R* are associated with increased risk of developing psoriasis (15–17).

Although it is not yet known what triggers dendritic cells to produce IL-23 in individuals predisposed to develop psoriasis, it is well established that IL-23 is a central growth factor for Th17 cells as it influences both their differentiation and expansion (18–20). Th17 cytokines, principally IL-17A and IL-22, exert profound effects on keratinocytes (21). In psoriasis lesions, keratinocytes are activated and proliferate at substantially faster rates than normal keratinocytes (22). IL-17A has been shown to induce cytokine and chemokine production by keratinocytes, but has not been shown to directly induce keratinocyte proliferation (8, 21, 23). By contrast, IL-22 induces antimicrobial peptide production by keratinocytes and is a direct potent stimulator of keratinocyte growth (12, 21, 24–26).

Studies using mice with varied genetic backgrounds have provided important insights into how IL-23 mediates skin pathology. Injection of recombinant murine (rm)IL-23 into skin of wild-type (WT) mice induces epidermal hyperplasia (3, 27). IL-23, however, fails to induce epidermal hyperplasia when injected into skin of *IL-22*$^{-/-}$ mice (25), which establishes IL-22 as a key downstream mediator of tissue effects caused by IL-23. IL-23–mediated epidermal hyperplasia is also dependent on CCR6, a chemokine receptor used by Th17 cells to migrate into skin (28). Although IL-17A does not directly induce keratinocyte growth in vitro, this cytokine likely plays a significant role in IL-23–induced skin pathology in vivo. Regarding this issue, Chan et al. (3) administered anti–IL-17A Abs prior to rmIL-23 injections into murine skin, but they did not detect decreases in epidermal hyperplasia. In this study, utilizing both *IL-17A*$^{-/-}$ mice and Ab blocking experiments, we demonstrate a critical role for IL-17A in mediating psoriasis-like epidermal hyperplasia that occurs following rmIL-23 injections into murine skin.

Materials and Methods

Animals

The Portland Veterans Affairs Medical Center Institutional Animal Care and Use Committee reviewed and approved all breeding and experiments. *IL-22*$^{-/-}$ mice were a kind gift from Dr. Ouyang Wenjun, Genentech (25), and *IL-17A*$^{-/-}$ mice were a kind gift from Dr. Yoichiro Iwakura, Center

*Department of Dermatology, Oregon Health & Science University, Portland, OR 97239; †Department of Biomedical Engineering, Oregon Health & Science University, Portland, OR 97239; ‡Dermatology Service, Veterans Affairs Medical Center, Portland, OR 97239; and §Department of Molecular Microbiology & Immunology, Oregon Health & Science University, Portland, OR 97239

[1]H.L.R. and S.K. contributed equally to this work.

Received for publication April 1, 2010. Accepted for publication November 23, 2010.

This work was supported in part by a Veterans Affairs Merit award (to A.B.), National Institutes of Health Grants 1 R21 AR054495-01A1 (to A.B.) and CA069533 (to K.G.P.), the Naito Foundation (to S.E.K.), and the National Institutes of Health under Ruth L. Kirschstein National Research Service Award 5-T32 CA106195-05 (to K.G.P.).

Address correspondence and reprint requests to Dr. Andrew Blauvelt, Oregon Health & Science University, 3303 SW Bond Avenue, CHD16, Portland, OR 97239. E-mail address: blauvean@ohsu.edu

The online version of this article contains supplemental material.

Abbreviations used in this article: qRT-PCR, quantitative RT-PCR; rCSLM, reflectance mode confocal scanning laser microscopy; rm, recombinant murine; WT, wild-type.

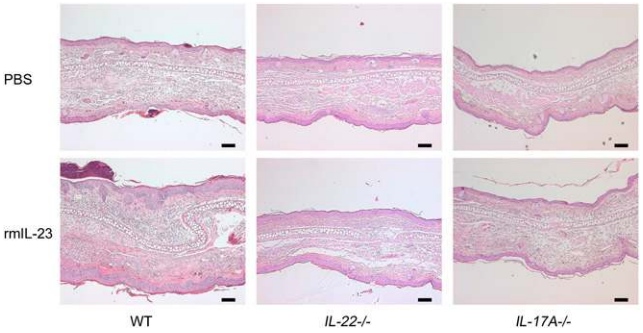

FIGURE 1. rmIL-23 induces epidermal hyperplasia in WT mice, but not in *IL-22*$^{-/-}$ or *IL-17A*$^{-/-}$ mice. Representative H&E-stained skin sections of ears from WT mice, *IL-22*$^{-/-}$ mice, and *IL-17A*$^{-/-}$ mice are shown following four daily injections of either rmIL-23 or PBS. Ten mice from each strain and condition were examined in three separate experiments. Scale bars, 0.1 mm.

for Experimental Medicine, Institute of Medical Science, University of Tokyo (29). Prior to using the mice, *IL-22*$^{-/-}$ mice and *IL-17A*$^{-/-}$ mice were backcrossed to C57BL/6 for six and eight generations, respectively. C57BL/6 wild-type mice were purchased from The Jackson Laboratory (Bar Harbor, ME). Mouse strains were evaluated to assure proper genotype by analyzing DNA isolated from tail snips at 4 wk of age and purified using DNeasy Blood and Tissue Kit (Qiagen, Valencia, CA). DNAs were genotyped by PCR amplification using PuReTaq Ready-To-Go PCR beads (GE Healthcare, Piscataway, NJ) and locus specific primers. Primer sequences and product sizes (in bp) are as follows: *IL-22* common forward 5′-CTCAGACCTCTACAGACAATCATC-3′ with WT specific reverse 5′-CAGCTGGCGGCCAAAGTCCC-3′ (196 bp) and mutant specific reverse 5′-GATACAGGTGCAGCTAAGCGAG-3′ (374 bp); *IL-17A* common forward 5′-ACTCTTCATCCACCTCACACGA-3′ with WT specific reverse 5′-CAGCATCAGAGACTAGAAGGGA-3′ (1.3 kb) and mutant specific reverse 5′-GCCATGATATAGACGTTGTGGC-3′ (500 bp). The annealing temperature was 56˚C for *IL-22* primers and 58˚C for *IL-17A* primers.

Intradermal cytokine injections

Mouse ears were injected intradermally with 20 μl PBS/0.1% BSA into one ear and 1 μg rmIL-23 (eBioscience, San Diego, CA) in PBS/0.1% BSA into the contralateral ear. Injections were continued in this manner daily for 4 d (days 0, 1, 2, and 3). For the Ab blocking experiments, 100 μg anti–IL-17A Abs (eBioscience), 50 μg anti–IL-22 Abs (eBioscience), 100 μg mouse IgG1 (eBioscience), or 50 μg rat IgG2a (eBioscience) were injected i.p. 1 h before injections into ear skin on days 0 and 2. Ear thickness was measured on day 4 using a G-1A dial thickness gauge (Peacock, Japan) by an observer blinded to treatment conditions and mouse genotype. Mice were then used for noninvasive confocal imaging, immunohistochemistry, or extraction of RNA.

Confocal imaging

Mice were placed in the supine position on a heated optical stage so that the ventral side of their ears could be imaged through a metal plate with a 3-mm diameter hole. The reflectance profile from the center of each ear was resolved using confocal detection through the 3-mm hole. During imaging, mice were anesthetized using vaporized isoflurane. Their breathing rates were regulated by providing 0.2 l/min oxygen and 0.8 l/min air mixed with the isoflurane vapor (1.5% v/v at 1 ATM). To restrict movement of the tissue

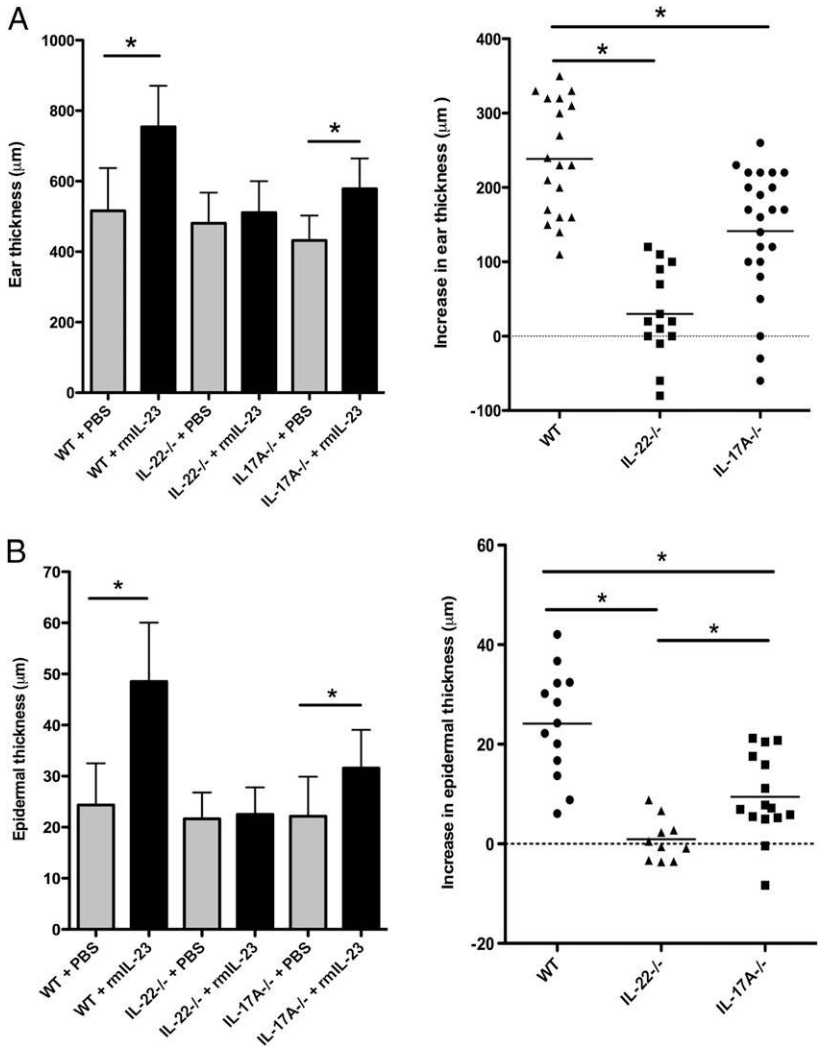

FIGURE 2. IL-23–induced epidermal hyperplasia is dependent on IL-22 and IL-17A. *A*, Gross ear thickness following four daily injections of rmIL-23 or PBS as measured using a caliper by an investigator blinded to the treatment conditions and genotypes of the mice. *B*, Epidermal hyperplasia following four daily injections of rmIL-23 or PBS using microscopic measurements on H&E-stained skin sections. Data are expressed as mean ± SD in bar graphs. Each dot indicates single specimen, and horizontal bars denote the mean of scatter plots. At least 10 mice from each strain and condition were studied in at least four separate experiments. For ear thickness of PBS- or rmIL-23–injected WT mice, data were analyzed using the Wilcoxon signed-rank test, because they were not normally distributed. All other data were analyzed with the paired *t* test, because they were normally distributed. *$p < 0.001$.

volume under investigation, the ear of the mouse was secured by placing a coverslip on the dorsal side of the ear.

Mouse imaging was performed using reflectance mode confocal scanning laser microscopy (rCSLM). The rCSLM system consists of an argon ion laser, λ = 488 nm, with an average output power of 10 mW, providing illumination through a water-coupled objective lens with numerical aperture 0.90 and magnfication ×60 (Olympus America, Melville, NY). The objective lens was set up in an inverted orientation. (x, y) translation of the focus was achieved using a scanning assembly consisting of two galvanometer mirrors (Nutfield Technology, Windham, NH) and a pair of relay lenses that directed the laser beam into the rear of the objective lens at varying angles. Confocal detection of light originating from the focus in the mouse tissue was achieved by recollimating the reflected signal and then returning the signal through the optical train until the beam was redirected by a beam-splitter toward a lens/pinhole/photo multiplier tube assembly. The z position of the sequential (x, y) scans was incremented in 1-μm steps by computer control of the translation stage. The spatial resolution along the x and y directions is 0.4 μm; z resolution is 1 μm. Data were acquired using an A/D converter controlled by Labview software (National Instruments, Austin, TX), and image reconstruction was conducted using Matlab software (The Mathworks, Natick, MA).

The confocal microscope records a three-dimensional image volume. These are a collection of images stacked along the z direction. "z" measures depth into the tissue. This image volume is divided into rectangular cubes (regions of interest) of size 10 pixels × 10 pixels × 100 pixels. In each region of interest, we average over all of the x, y locations to yield an average reflectance profile, or brightness of the reflected light as a function of depth. This reflected brightness has two local maxima: one at the tissue–water interface (stratum corneum) and one in the upper dermis. The peaks are a result of the tissue–light interaction. The dermal–epidermal junction corresponds to the local minima between the two peaks (it appears as a dark fringe in the sagittal confocal images). The thickness of the epidermis was determined by taking the average distance between the first reflective surface (the beginning of the stratum corneum) in the confocal images to the dark fringe before the second reflective surface (the upper dermis) in 2500 regions of interest (30).

Histology and immunohistochemistry

Sections from formalin-fixed, paraffin-embedded ears were stained with H&E, and epidermal thickness was measured using ImagePro Plus software (Leeds Precision Instruments, Minneapolis, MN). With this software, the epidermis was outlined for each tissue section using a series of rectangles, and the total epidermal area was determined. Thickness was then calculated as a measure of total area divided by total length of the epidermis. For immunohistochemistry, sections were deparaffinized and hydrated by washing sections in xylene followed by a graded alcohol series. To unmask Ags, sections were incubated in 10 mM citric acid (pH 6) at 95°C for 30 min, and endogenous peroxidase activity was quenched by treating sections with 3% hydrogen peroxide for 5 min at room temperature. Sections were blocked for 60 min at room temperature followed by incubation with primary Abs overnight at 4°C. Samples were washed and incubated for 60 min with secondary Abs and developed using Vectastain Elite ABC kit (Vector Laboratories, Burlingame, CA) and DAB substrate kit for peroxidase (Vector Laboratories). All stained sections were counterstained with hematoxylin (Vector Laboratories). Blocking solutions, primary Abs, and secondary Abs used are shown in Supplemental Table I. Sections from at least three mice per group were stained, and photomicrographs were taken of representative ×40 magnification fields. Average numbers of positive cells per photomicrograph were counted.

RNA isolation and quantitative real-time RT-PCR

Injected ears were collected, placed in TRIzol (Invitrogen), and homogenized with a mechanical rotor for 1 min. Total RNA was isolated and purified using TRIzol and the PureLink RNA Mini Kit (Invitrogen) as recommended by the manufacturer. cDNA was prepared from 1 μg total RNA by reverse transcription using a High-Capacity cDNA Reverse Transcription Kit (Applied Biosystems). Reactions were diluted three times with RNase-free water for all quantitative RT-PCR (qRT-PCR) experiments. qRT-PCR was performed using TaqMan Gene Expression Master Mix with TaqMan primers and fluorescent probes from Applied Biosystems for *Gapdh* (catalog no. Mm99999915_g1), *il17a* (catalog no. Mm01268754_m1), *Il22* (catalog no. Mm01226722_g1), *Ifnγ* (catalog no. Mm00801778_m1), *Il17f* (catalog no. Mm00521423_m1), *Il21* (catalog no. Mm00517640_m1), and *Tnfα* (catalog no. Mm00443258_m1) on the MyiQ system (Bio-Rad). Expression of each transcript was calculated relative to *Gapdh*. Fold change relative to the PBS-injected ear was calculated using the $2^{\Delta\Delta Ct}$ method, where $\Delta Ct = Ct_{cytokine} - Ct_{GAPDH}$ and $\Delta\Delta Ct = \Delta Ct_{PBS\text{-}injected} - \Delta Ct_{rmIL\text{-}23\text{–}injected}$.

Statistical analyses

The χ^2 goodness-of-fit test was used to evaluate normality for all parameters. The F test and Bartlett test were used to evaluate equality of variance between two and three groups, respectively. Welch's t test was used for analysis of mRNA expression between different strains of mice. Statistical analyses for comparison of PBS-injected ears and rmIL-23–injected ears were performed using the paired t test or Wilcoxon signed-rank test. For testing equality of population medians among rmIL-23–injected WT, *IL-17A*$^{-/-}$, and *IL-22*$^{-/-}$ mice, Kruskal-Wallis test and Scheffe's F test were used. p values of 0.05 or less were considered significant.

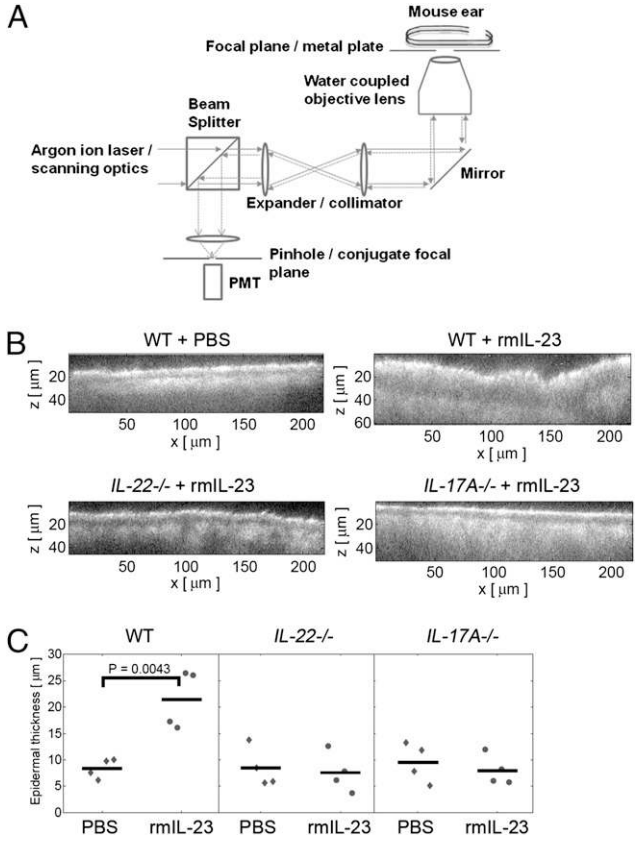

FIGURE 3. *A*, Schematic of noninvasive confocal imaging device. Illuminating rays are solid; the reflected rays from the sample plane are dotted. The rCSLM system consists of an argon ion laser, λ = 488 nm, a water-coupled objective lens with numerical aperture (NA) 0.90 and ×60 magnification. Translation of the focus was achieved using a scanning assembly consisting of two galvanometer mirrors and a pair of relay lenses. Confocal detection of light was achieved by collimating the reflected signal and redirecting the beam toward a lens/pinhole/photo multiplier tube assembly. Mice were placed in the supine position so that the dorsal side of their ears could be imaged. *B*, Representative sagittal rCSLM reflectance views of the epidermis and upper dermis of mice. The top white surface in each image corresponds to the stratum corneum followed by a darker region, which is the dermal–epidermal junction. The second reflective surface is the upper dermis. *C*, Epidermal hyperplasia of WT mice, *IL-17A*$^{-/-}$ mice, and *IL-22*$^{-/-}$ mice following four daily injections of either rmIL-23 or PBS. WT mice demonstrated the greatest degree of epidermal hyperplasia in response to rmIL-23 when compared with saline ($p < 0.006$), whereas *IL-22*$^{-/-}$ mice and *IL-17A*$^{-/-}$ exhibited little to no epidermal thickening ($p < 0.75$ and $p < 0.55$, respectively). Each dot indicates a single specimen; horizontal bars indicate mean. Four mice from each strain and condition were studied in four separate experiments. Scatter graphs were analyzed with the paired t test.

Results

IL-23–induced epidermal hyperplasia is dependent on IL-22 and IL-17A

H&E staining of ear sections showed that rmIL-23–injected WT mice had thicker ears and increased infiltration of inflammatory cells within the dermis when compared with saline-injected skin (Fig. 1). Gross ear thickness, as measured in live mice with a caliper by an investigator blinded to the genotypes and treatment conditions of the mice, was also greater in rmIL-23–injected WT mice when compared with saline-injected WT mice ($p < 0.001$) (Fig. 2*A*). In addition, epidermal hyperplasia (i.e., acanthosis) as mea-

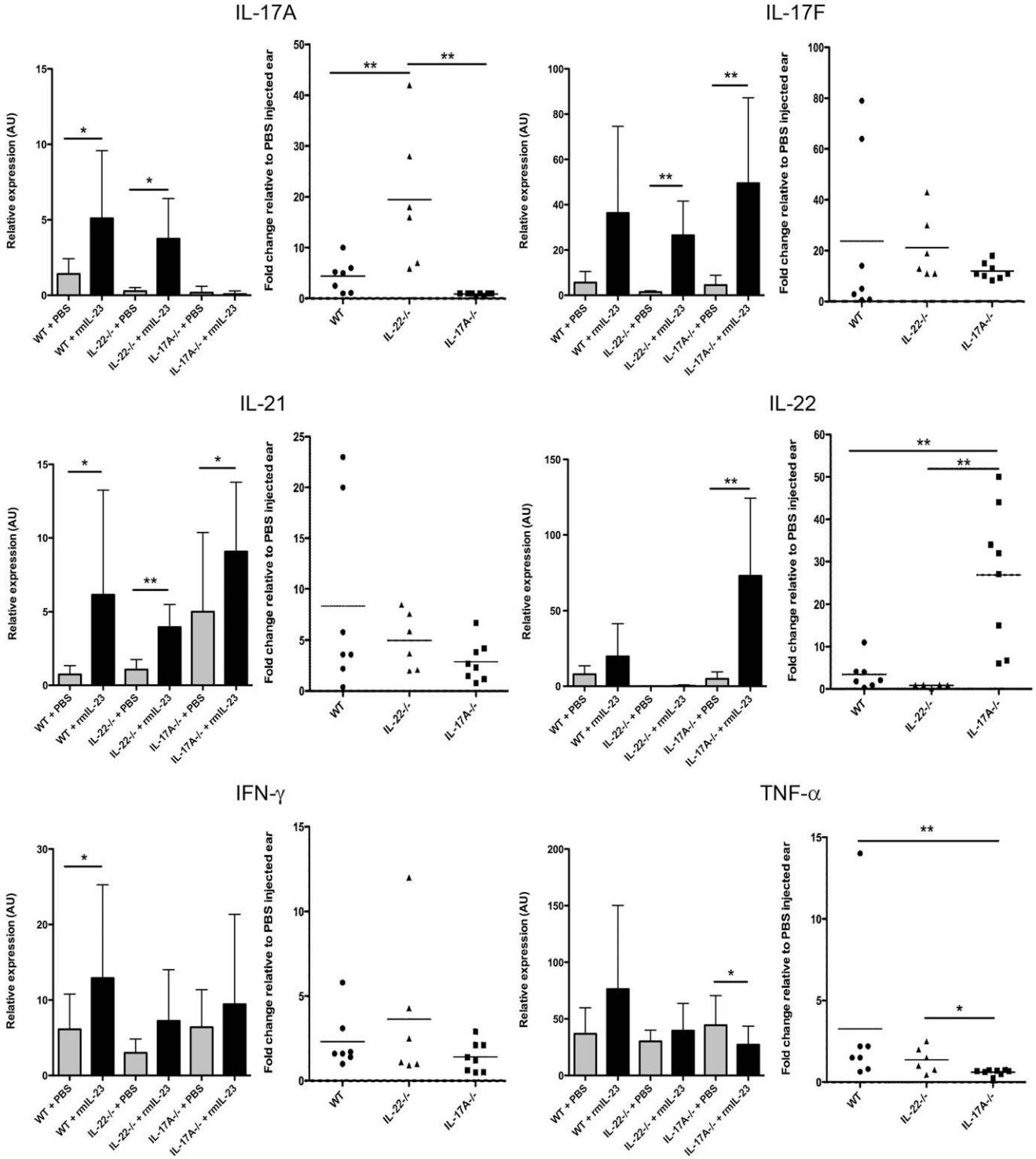

FIGURE 4. IL-17A or IL-22 alone is not sufficient to cause IL-23–mediated epidermal hyperplasia. Bar graphs show relative mRNA expression of *IL-17A*, *IL-17F*, *IL-21*, *IL-22*, *IFN-γ*, and *TNF-α* in rmIL-23–injected and PBS-injected WT mice, *IL-22*$^{-/-}$ mice, and *IL-17A*$^{-/-}$ mice. Scatter graphs show fold change in mRNA expression of these cytokines in rmIL-23–injected ears relative to PBS-injected ears in WT mice, *IL-22*$^{-/-}$ mice, and *IL-17A*$^{-/-}$ mice. Data are expressed as mean ± SD in bar graphs. Each dot indicates single specimen, and horizontal bars denote the mean of scatter plots. At least six mice from each strain and condition were studied in at least three separate experiments. Bar graphs were analyzed using the Wilcoxon signed-rank test (when not normally distributed) or paired *t* test (when normally distributed). Scatter graphs were analyzed using the Kruskal-Wallis test and Scheffe's *F* test. *$p < 0.05$; **$p < 0.01$. AU, arbitrary units.

sured by H&E staining was greater in rmIL-23–injected WT mice when compared with saline-injected WT mice ($p < 0.001$) (Figs. 1, 2*B*). Using novel noninvasive confocal microscopy in live animals, epidermal thickness was also prominently demonstrated in rmIL-23–injected ears of WT mice versus saline-injected WT mice ($p < 0.004$) (Fig. 3). Other histologic changes, including hyperkeratosis, parakeratosis, spongiosis, subcorneal collections of neutrophils, and increased numbers and dilation of blood vessels, were not observed 4 d following daily injections of rmIL-23 in WT mice (Fig. 1).

Consistent with a previous report (25), thickness of ears and epidermis were comparable in rmIL-23–injected *IL-22*$^{-/-}$ mice when compared with saline-injected *IL-22*$^{-/-}$ mice ($p < 0.09$ for ear thickness; $p < 0.51$ for epidermal thickness by histology; and $p < 0.75$ for epidermal thickness by confocal) (Figs. 1–3). rmIL-23–injected *IL-22*$^{-/-}$ mice had significantly thinner ears and epidermis when compared with rmIL-23–injected WT mice ($p < 0.001$ for ear thickness; $p < 0.001$ for epidermal thickness by histology; and $p < 0.006$ for epidermal thickness by confocal microscopy) (Figs. 1–3). When using rCSLM to measure epidermal thickness, rmIL-23–injected skin of *IL-17A*$^{-/-}$ mice showed no statistically significant epidermal thickness when compared with saline-injected skin of *IL-17A*$^{-/-}$ mice ($p < 0.55$). Utilizing other measurement techniques, thickness of ears and epidermis were increased in rmIL-23–injected *IL-17A*$^{-/-}$ mice when compared with saline-injected *IL-17A*$^{-/-}$ mice ($p < 0.001$ for ear thickness; $p < 0.001$ for epidermal thickness by histology) (Figs. 1–3). Notably, however, rmIL-23–injected *IL-17A*$^{-/-}$ mice had significantly thinner ears and epidermis when compared with rmIL-23–injected WT mice by all methods ($p < 0.001$ for ear thickness; $p < 0.001$ for epidermal thickness by histology; and $p < 0.005$ for epidermal thickness by confocal microscopy) (Figs. 1–3). rmIL-23–injected *IL-22*$^{-/-}$ mice had thinner epidermis when compared with rmIL-23–injected *IL-17A*$^{-/-}$ mice by histology ($p < 0.001$), but the difference in total ear thickness of these mice was not statistically significant ($p < 0.063$) (Figs. 1, 2). As in the WT mice, other histologic features, such as hyperkeratosis, parakeratosis, spongiosis, subcorneal collections of neutrophils, and increased numbers and dilation of blood vessels, were not observed in any of the knockout mice (Fig. 1).

Neither IL-17A nor IL-22 alone is sufficient to cause IL-23–mediated epidermal hyperplasia

To characterize immune responses within rmIL-23–injected skin, expression of cytokines was measured by real-time qRT-PCR. In WT mice, injections of rmIL-23 induced *IL-17A* mRNA expression when compared with saline-injected WT mice ($p < 0.05$), but *IL-22* mRNA induction was not statistically significant ($p < 0.15$) (Fig. 4). In *IL-22*$^{-/-}$ mice, *IL-22* mRNA was not expressed, and there was greater fold induction of *IL-17A* mRNA by rmIL-23 compared with rmIL-23–injected WT mice ($p < 0.05$) (Fig. 4). Conversely, in *IL-17A*$^{-/-}$ mice, *IL-17A* mRNA was not expressed, and *IL-22* mRNA was induced by rmIL-23 to levels higher than those seen in rmIL-23–injected WT mice ($p < 0.01$) (Fig. 4). In addition, rmIL-23 induced absolute levels of *TNF-α* mRNA similarly in all strains of mice, but fold induction of *TNF-α* mRNA in *IL-17A*$^{-/-}$ mice was significantly lower than that in WT mice ($p < 0.05$) (Fig. 4). In fact, in all eight *IL-17A*$^{-/-}$ mice studied, rmIL-23 induced lesser *TNF-α* mRNA expression than saline. It is possible that this relative decrease in inducible *TNF-α* mRNA in *IL-17A* knockout mice may contribute to the lack of epidermal hyperplasia seen in these mice following rmIL-23 injections. We also measured rmIL-23–induced mRNA expression of *IFN-γ*, *IL-17F*, and *IL-21*; however, there were no significant differences in absolute expression or in fold induction of these genes between the different strains of mice used in this study (Fig 4). Thus, these data suggest that rmIL-23–induced levels of IL-17F, IL-21, and IFN-γ were not sufficient to cause epidermal hyperplasia in our experiments.

Confirmation of *IL-17A* and *IL-22* mRNA results was performed via protein analyses using immunohistochemistry. Both IL-17A^{+} and IL-22^{+} cells were readily observed in the dermis of rmIL-23–injected WT skin (Fig. 5). IL-17A^{+} cells, but not IL-22^{+} cells, were also readily apparent in the dermis of *IL-22*$^{-/-}$ mice injected with rmIL-23, whereas IL-22^{+} cells, but not IL-17A^{+} cells, were readily visualized in the dermis of *IL-17A*$^{-/-}$ mice injected with rmIL-23 (Figs. 5, 6*A*). Thus, the combined mRNA and protein analyses revealed that IL-22 was present, if not elevated, in *IL-17A*$^{-/-}$ mice and that IL-17A levels were normal to elevated in *IL-22*$^{-/-}$ mice. These data suggest that neither cytokine alone is sufficient to mediate IL-23–induced epidermal changes. In other words, both of these cytokines are critical for this process to occur.

Characterization of cutaneous leukocyte populations following injections with rmIL-23

To localize and quantify leukocyte populations in skin following injections of rmIL-23, we performed immunohistochemistry for CD3 (T cells), CD11c (dendritic cells), F4/80 (macrophages), and Gr-1 (neutrophils). *IL-17A*$^{-/-}$ mice injected with rmIL-23 had more F4/80^{+} cells and Gr-1^{+} cells when compared with *IL-22*$^{-/-}$ mice injected with rmIL-23 ($p < 0.01$ and $p < 0.05$, respectively) (Figs. 5, 6*A*). There were no differences, however, in F4/80^{+} or Gr-1^{+} cells between WT mice and *IL-17A*$^{-/-}$ or *IL-22*$^{-/-}$ mice. CD3^{+} T cells were decreased in both *IL-17A*$^{-/-}$ and *IL-22*$^{-/-}$

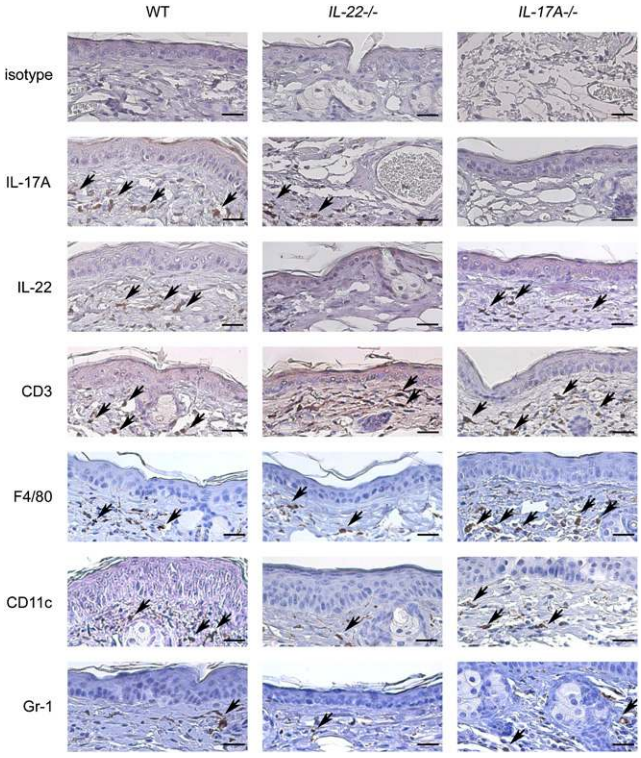

FIGURE 5. rmIL-23 induces IL-17A expression in WT and *IL-22*$^{-/-}$ mice and IL-22 expression in WT and *IL-17A*$^{-/-}$ mice. Representative sections of rmIL-23–injected ears from WT mice, *IL-17A*$^{-/-}$ mice, and *IL-22*$^{-/-}$ mice following 4 d of injections were stained with various Abs (see Supplemental Table I). Sections from three mice from each strain were examined in three separate experiments. Scale bars, 0.025 mm. Black arrows indicate positively stained cells.

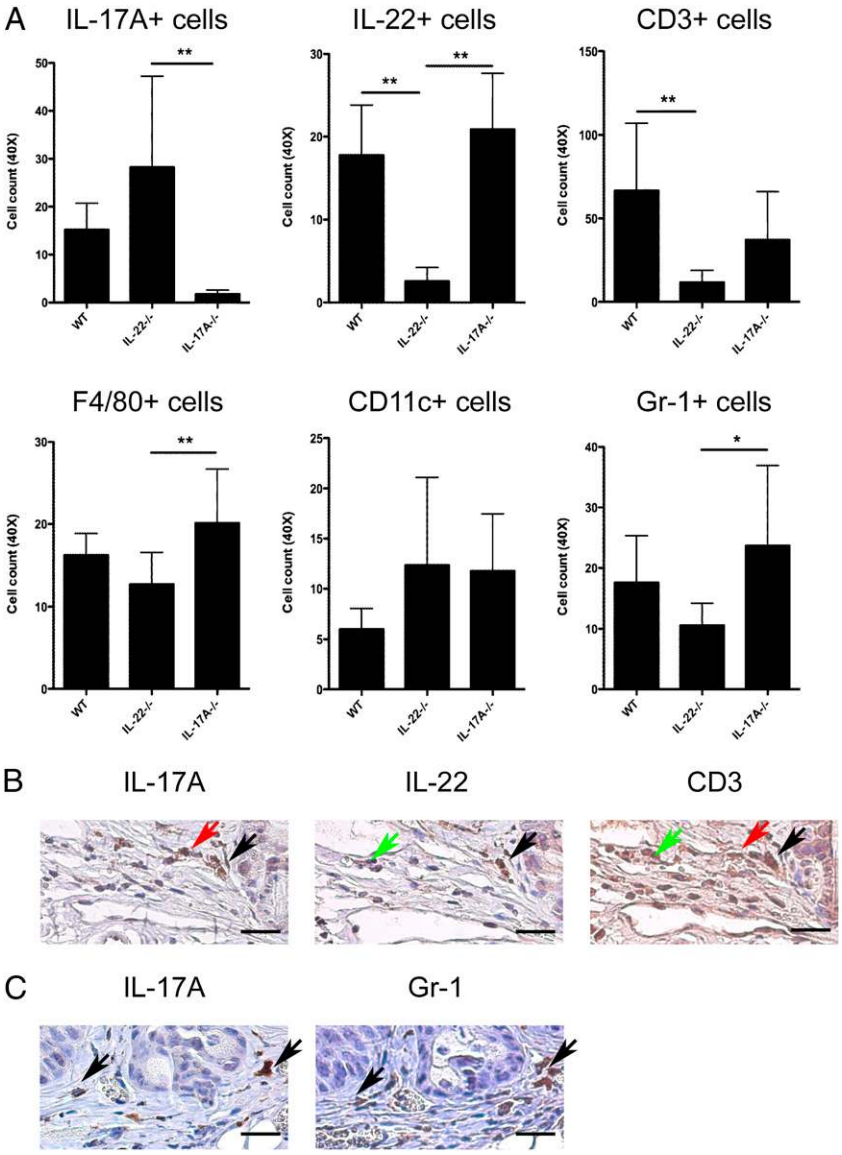

FIGURE 6. IL-17A is mainly produced by $CD3^+$ T cells and Gr-1^+ neutrophils, and IL-22 is mainly produced by $CD3^+$ T cells. *A*, Quantification of positively stained cells in each of the three groups of mice shown in Fig. 5. Bar graphs were analyzed with Kruskal-Wallis test and Scheffe's *F* test. IL-17A, IL-22, and CD3 (*B*) or IL-17A and Gr-1 (*C*) staining of representative serial sections of WT mice skin following four daily injections of rmIL-23. Sections from three WT mice were examined in two separate experiments. Scale bars, 0.025 mm. Black arrows indicate triple-positive cells (in *B*) and double-positive cells (in *C*), green arrows indicate $CD3^+IL\text{-}17A^+IL\text{-}22^-$ cells, and red arrows indicate $CD3^+IL\text{-}17A^-IL\text{-}22^+$ cells. $*p < 0.05$; $**p < 0.01$.

mice compared with WT mice, although differences were only statistically significant for *IL-22*$^{-/-}$ mice (Figs. 5, 6*A*). Next, we stained serial sections to detect double-positive cells. IL-17A was mainly produced by $CD3^+$ T cells (Fig. 6*B*), whereas some Gr-1^+ cells also produced IL-17A (Fig. 6*C*). IL-22 was also primarily produced by $CD3^+$ T cells (Fig. 6*B*). Some, but not all, IL-$17A^+$ cells were also IL-22^+ (Fig. 6*B*).

Pretreatment with blocking Abs directed against either IL-22 or IL-17A inhibit epidermal hyperplasia induced by rmIL-23 injections into skin

To confirm and extend our studies in genetic knockout mice, we injected WT mice with anti–IL-22 Abs, anti–IL-17A Abs, or isotype control Abs 1 h before rmIL-23 injections on days 0 and 2. Pretreatment with either anti–IL-22 Abs or anti–IL-17A Abs completely blocked induction of epidermal hyperplasia by rmIL-23 (Fig. 7). This result is consonant with findings in our genetic knockout mice that support a critical role for IL-17A, like IL-22, as a downstream mediator of IL-23–induced skin pathology.

Discussion

IL-23 and Th17 cells play a central role in psoriasis pathogenesis (1). IL-23 is predominantly produced by inflammatory dendritic cells in the dermis of skin affected by psoriasis (2, 5–7). Experiments in which rmIL-23 is injected into skin of mice have provided useful information regarding the mechanisms involved in IL-23–induced psoriasiform inflammation in skin (3, 25, 28). In this study, a central role for IL-17A in mediating downstream effects of IL-23 in murine skin is demonstrated, to our knowledge, for the first time. Specifically, mice deficient in IL-17A demonstrated little epidermal hyperplasia following repeated injections of rmIL-23 into skin (Figs. 1–3), and WT mice treated with anti–IL-17A Abs showed no IL-23–induced epidermal hyperplasia (Fig. 7). This IL-17A finding is analogous to a prior report (and confirmatory findings shown in this study) that IL-22 is a critical downstream mediator of IL-23–induced epidermal hyperplasia (25). Because IL-22 has a direct proliferative effect on keratinocytes (12, 21, 24–26), whereas IL-17A does not (8, 21, 23), the in vivo role for IL-17A in promoting epidermal hyperplasia is

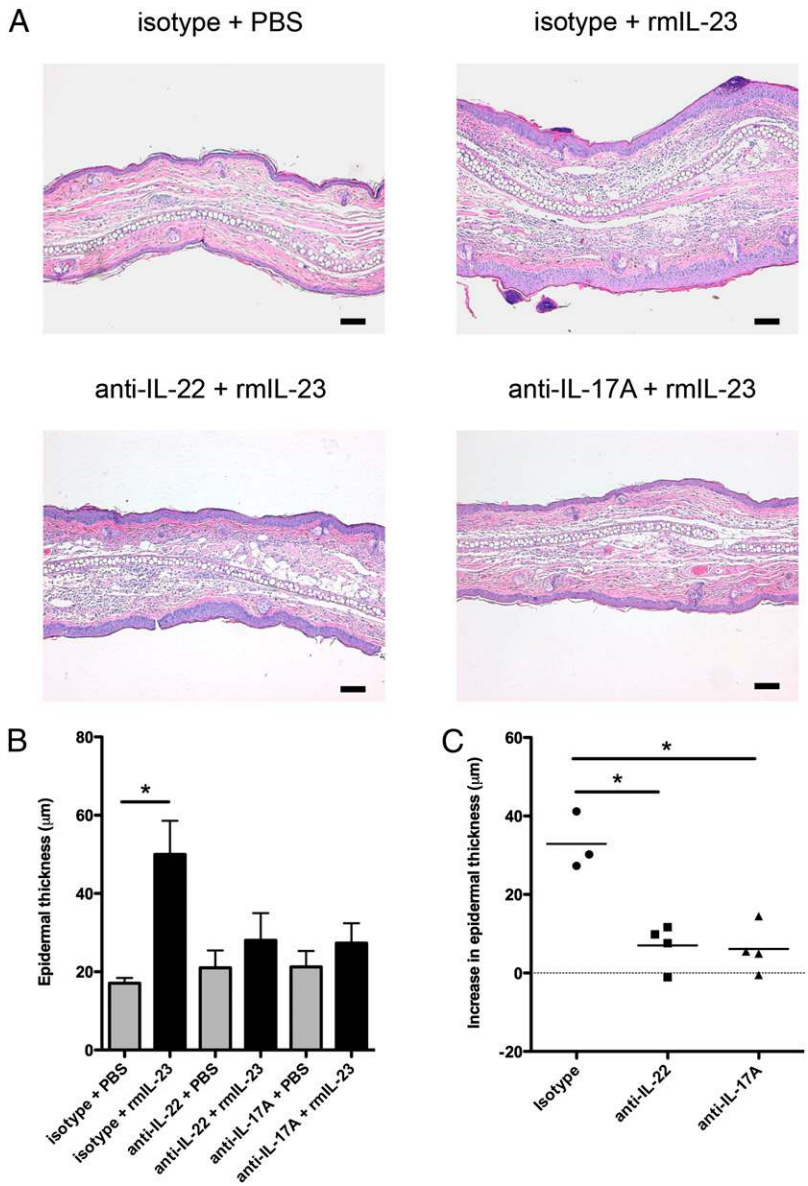

FIGURE 7. Both anti–IL-22 Abs and anti–IL-17A Abs block develop of epidermal hyperplasia in WT skin following injections of rmIL-23. *A*, Representative H&E-stained skin sections of ears from WT mice are shown following four daily injections of either rmIL-23 or PBS. As indicated, anti–IL-22 Abs ($n = 4$), anti–IL-17A Abs ($n = 4$), or isotype Abs ($n = 3$) were injected i.p. 1 h prior to rmIL-23 injections on days 0 and 2 in two separate experiments. Scale bars, 0.1 mm. *B*, Epidermal hyperplasia as quantified by imaging software and microscopy on H&E-stained skin sections. Data are expressed as mean ± SD and analyzed with the paired *t* test. *C*, The change in epidermal thickness with each dot indicating a single mouse and horizontal bars denoting the mean of the scatter plots. Scatter graphs were analyzed using the Kruskal-Wallis test and Scheffe's *F* test. $*p < 0.001$.

likely due to indirect effects on keratinocytes. For example, we showed that *TNF-α* mRNA was not induced in *IL-17A* knockout mice treated with rmIL-23 (Fig. 5), which could be playing a role in the failure to induce epidermal thickening. Additionally, IL-17A can induce CCL20 expression by keratinocytes and promote chemotaxis of $CCR6^+$ cells into skin (8); thus, IL-17A–deficient mice may demonstrate impaired movement of $CCR6^+$ Th17 cells, which is a critical component of IL-23–mediated psoriasiform inflammation (28). Of note, our Ab results differ from Chan et al. (3), who showed that anti–IL-17A Abs did not block psoriasiform changes in murine skin injected with rmIL-23. This discrepancy can possibly be explained by methodologic differences between these investigators and our laboratory regarding: 1) genetic background of the mice; 2) sources of anti–IL-17A Ab; and/or 3) treatment protocols.

A novel aspect of this report is the use of noninvasive confocal microscopy, or rCSLM, to measure epidermal thickening in live animals (Fig. 3). Findings from this imaging modality corroborated nicely with epidermal thickness measurements on histologic specimens obtained immediately after mice were sacrificed (Fig. 2*B*). rCSLM is a promising technique for use in live small animal imaging, as it provides a quantitative means of studying morphology associated with cutaneous disease in vivo (30). Applications to quantifying epidermal thickness in humans with skin disease are underway (31).

It is likely that other Th17 cytokines other than IL-17A and IL-22 are also critically involved in IL-23–mediated cutaneous pathology. On a technical note, we used an IL-23 injection model that assessed short-term effects of IL-23 on skin, like some others (3, 28), whereas other investigators have assessed IL-23–induced skin changes over longer periods of time (25). Caruso and colleagues (10) recently highlighted a key role for IL-21 in psoriasis-like keratinocyte hyperproliferation, although we did not observe differences in *IL-21* mRNA levels between WT and knockout mice in our experiments (Fig. 4). They found that blocking IL-22 did not prevent IL-21–induced epidermal thickening (10). In addition, members of the IL-10 family of cytokines other than IL-22, such as IL-19, IL-20, and IL-24, were reported to induce epidermal hyperplasia directly (26). rmIL-23 injections induced *IL-19* mRNA and *IL-24* mRNA, but not *IL-20* mRNA, and IL-23–induced epidermal hyperplasia was decreased in *IL-20R2*$^{-/-}$ mice, but not in *IL-19*$^{-/-}$ and *IL-24*$^{-/-}$ mice (3). Moreover, these investigators showed that TNF-α was induced by intradermal injection of rmIL-23

and that mAbs directed against TNF-α partially inhibited IL-23–dependent epidermal hyperplasia (3). This latter finding may partly explain the clinical efficacy of TNF-α blockade in individuals with psoriasis.

Clinical findings in psoriasis patients support the concept that IL-23 is critical in psoriasis pathogenesis. Thus far, the mAbs ustekinumab and briakinumab, directed against IL-12/23p40, have shown remarkable clinical efficacy in individuals with moderate-to-severe psoriasis (32–35). Several drugs that block only IL-23 (and not IL-12) target IL-23p19 and are currently in phase I and phase II development for psoriasis. In addition, mAbs and receptor antagonists that block either IL-17A or IL-22 function are also under development (36). A critical point shown in this study is that the presence of normal-to-increased levels of IL-22 in *IL-17A*$^{-/-}$ mice and the presence of normal-to-increased levels of *IL-17A* in *IL-22*$^{-/-}$ mice following rmIL-23 injections suggests that neither Th17 cytokine alone is sufficient to promote IL-23–induced psoriasis-like changes in murine skin (Figs. 4, 5). Because genetic and Ab targeting of either IL-17A or IL-22 leads to impaired IL-23–mediated immune responses in skin, these data support the use of drugs for psoriasis that block function of either IL-17A (36) or IL-22.

Disclosures

The authors have no financial conflicts of interest.

References

1. Di Cesare, A., P. Di Meglio, and F. O. Nestle. 2009. The IL-23/Th17 axis in the immunopathogenesis of psoriasis. *J. Invest. Dermatol.* 129: 1339–1350.
2. Lee, E., W. L. Trepicchio, J. L. Oestreicher, D. Pittman, F. Wang, F. Chamian, M. Dhodapkar, and J. G. Krueger. 2004. Increased expression of interleukin 23 p19 and p40 in lesional skin of patients with psoriasis vulgaris. *J. Exp. Med.* 199: 125–130.
3. Chan, J. R., W. Blumenschein, E. Murphy, C. Diveu, M. Wiekowski, S. Abbondanzo, L. Lucian, R. Geissler, S. Brodie, A. B. Kimball, et al. 2006. IL-23 stimulates epidermal hyperplasia via TNF and IL-20R2-dependent mechanisms with implications for psoriasis pathogenesis. *J. Exp. Med.* 203: 2577–2587.
4. Zaba, L. C., I. Cardinale, P. Gilleaudeau, M. Sullivan-Whalen, M. Suárez-Fariñas, M. Suárez-Fariñas, J. Fuentes-Duculan, I. Novitskaya, A. Khatcherian, M. J. Bluth, et al. 2007. Amelioration of epidermal hyperplasia by TNF inhibition is associated with reduced Th17 responses. [Published erratum appears in 2008 *J. Exp. Med.* 205: 1941.] *J. Exp. Med.* 204: 3183–3194.
5. Piskin, G., R. M. Sylva-Steenland, J. D. Bos, and M. B. Teunissen. 2006. In vitro and in situ expression of IL-23 by keratinocytes in healthy skin and psoriasis lesions: enhanced expression in psoriatic skin. *J. Immunol.* 176: 1908–1915.
6. Wilson, N. J., K. Boniface, J. R. Chan, B. S. McKenzie, W. M. Blumenschein, J. D. Mattson, B. Basham, K. Smith, T. Chen, F. Morel, et al. 2007. Development, cytokine profile and function of human interleukin 17-producing helper T cells. *Nat. Immunol.* 8: 950–957.
7. Lillis, J. V., C. S. Guo, J. J. Lee, and A. Blauvelt. 2010. Increased IL-23 expression in palmoplantar psoriasis and hyperkeratotic hand dermatitis. *Arch. Dermatol.* 146: 918–919.
8. Harper, E. G., C. Guo, H. Rizzo, J. V. Lillis, S. E. Kurtz, I. Skorcheva, D. Purdy, E. Fitch, M. Iordanov, and A. Blauvelt. 2009. Th17 cytokines stimulate CCL20 expression in keratinocytes in vitro and in vivo: implications for psoriasis pathogenesis. *J. Invest. Dermatol.* 129: 2175–2183.
9. Johansen, C., P. A. Usher, R. B. Kjellerup, D. Lundsgaard, L. Iversen, and K. Kragballe. 2009. Characterization of the interleukin-17 isoforms and receptors in lesional psoriatic skin. *Br. J. Dermatol.* 160: 319–324.
10. Caruso, R., E. Botti, M. Sarra, M. Esposito, C. Stolfi, L. Diluvio, M. L. Giustizieri, V. Pacciani, A. Mazzotta, E. Campione, et al. 2009. Involvement of interleukin-21 in the epidermal hyperplasia of psoriasis. *Nat. Med.* 15: 1013–1015.
11. Lowes, M. A., T. Kikuchi, J. Fuentes-Duculan, I. Cardinale, L. C. Zaba, A. S. Haider, E. P. Bowman, and J. G. Krueger. 2008. Psoriasis vulgaris lesions contain discrete populations of Th1 and Th17 T cells. *J. Invest. Dermatol.* 128: 1207–1211.
12. Wolk, K., E. Witte, E. Wallace, W. D. Döcke, S. Kunz, K. Asadullah, H. D. Volk, W. Sterry, and R. Sabat. 2006. IL-22 regulates the expression of genes responsible for antimicrobial defense, cellular differentiation, and mobility in keratinocytes: a potential role in psoriasis. *Eur. J. Immunol.* 36: 1309–1323.
13. Boniface, K., E. Guignouard, N. Pedretti, M. Garcia, A. Delwail, F. X. Bernard, F. Nau, G. Guillet, G. Dagregorio, H. Yssel, et al. 2007. A role for T cell-derived interleukin 22 in psoriatic skin inflammation. *Clin. Exp. Immunol.* 150: 407–415.
14. Kagami, S., H. L. Rizzo, J. J. Lee, Y. Koguchi, and A. Blauvelt. 2010. Circulating Th17, Th22, and Th1 cells are increased in psoriasis. *J. Invest. Dermatol.* 130: 1373–1383.
15. Capon, F., P. Di Meglio, J. Szaub, N. J. Prescott, C. Dunster, L. Baumber, K. Timms, A. Gutin, V. Abkevic, A. D. Burden, et al. 2007. Sequence variants in the genes for the interleukin-23 receptor (IL23R) and its ligand (IL12B) confer protection against psoriasis. *Hum. Genet.* 122: 201–206.
16. Cargill, M., S. J. Schrodi, M. Chang, V. E. Garcia, R. Brandon, K. P. Callis, N. Matsunami, K. G. Ardlie, D. Civello, J. J. Catanese, et al. 2007. A large-scale genetic association study confirms IL12B and leads to the identification of IL23R as psoriasis-risk genes. *Am. J. Hum. Genet.* 80: 273–290.
17. Nair, R. P., K. C. Duffin, C. Helms, J. Ding, P. E. Stuart, D. Goldgar, J. E. Gudjonsson, Y. Li, T. Tejasvi, B. J. Feng, et al; Collaborative Association Study of Psoriasis. 2009. Genome-wide scan reveals association of psoriasis with IL-23 and NF-kappaB pathways. *Nat. Genet.* 41: 199–204.
18. Miossec, P., T. Korn, and V. K. Kuchroo. 2009. Interleukin-17 and type 17 helper T cells. *N. Engl. J. Med.* 361: 888–898.
19. Romagnani, S., E. Maggi, F. Liotta, L. Cosmi, and F. Annunziato. 2009. Properties and origin of human Th17 cells. *Mol. Immunol.* 47: 3–7.
20. Korn, T., E. Bettelli, M. Oukka, and V. K. Kuchroo. 2009. IL-17 and Th17 Cells. *Annu. Rev. Immunol.* 27: 485–517.
21. Nograles, K. E., L. C. Zaba, E. Guttman-Yassky, J. Fuentes-Duculan, M. Suárez-Fariñas, I. Cardinale, A. Khatcherian, J. Gonzalez, K. C. Pierson, T. R. White, et al. 2008. Th17 cytokines interleukin (IL)-17 and IL-22 modulate distinct inflammatory and keratinocyte-response pathways. *Br. J. Dermatol.* 159: 1092–1102.
22. Iizuka, H. 1994. Epidermal turnover time. *J. Dermatol. Sci.* 8: 215–217.
23. Albanesi, C., C. Scarponi, A. Cavani, M. Federici, F. Nasorri, and G. Girolomoni. 2000. Interleukin-17 is produced by both Th1 and Th2 lymphocytes, and modulates interferon-gamma- and interleukin-4-induced activation of human keratinocytes. *J. Invest. Dermatol.* 115: 81–87.
24. Liang, S. C., X. Y. Tan, D. P. Luxenberg, R. Karim, K. Dunussi-Joannopoulos, M. Collins, and L. A. Fouser. 2006. Interleukin (IL)-22 and IL-17 are coexpressed by Th17 cells and cooperatively enhance expression of antimicrobial peptides. *J. Exp. Med.* 203: 2271–2279.
25. Zheng, Y., D. M. Danilenko, P. Valdez, I. Kasman, J. Eastham-Anderson, J. Wu, and W. Ouyang. 2007. Interleukin-22, a T(H)17 cytokine, mediates IL-23-induced dermal inflammation and acanthosis. *Nature* 445: 648–651.
26. Sa, S. M., P. A. Valdez, J. Wu, K. Jung, F. Zhong, L. Hall, I. Kasman, J. Winer, Z. Modrusan, D. M. Danilenko, and W. Ouyang. 2007. The effects of IL-20 subfamily cytokines on reconstituted human epidermis suggest potential roles in cutaneous innate defense and pathogenic adaptive immunity in psoriasis. *J. Immunol.* 178: 2229–2240.
27. Kopp, T., P. Lenz, C. Bello-Fernandez, R. A. Kastelein, T. S. Kupper, and G. Stingl. 2003. IL-23 production by cosecretion of endogenous p19 and transgenic p40 in keratin 14/p40 transgenic mice: evidence for enhanced cutaneous immunity. *J. Immunol.* 170: 5438–5444.
28. Hedrick, M. N., A. S. Lonsdorf, A. K. Shirakawa, C. C. Richard Lee, F. Liao, S. P. Singh, H. H. Zhang, A. Grinberg, P. E. Love, S. T. Hwang, and J. M. Farber. 2009. CCR6 is required for IL-23-induced psoriasis-like inflammation in mice. *J. Clin. Invest.* 119: 2317–2329.
29. Nakae, S., Y. Komiyama, A. Nambu, K. Sudo, M. Iwase, I. Homma, K. Sekikawa, M. Asano, and Y. Iwakura. 2002. Antigen-specific T cell sensitization is impaired in IL-17-deficient mice, causing suppression of allergic cellular and humoral responses. *Immunity* 17: 375–387.
30. Phillips, K. G., R. Samatham, N. Choudhury, J. C. Gladish, P. Thuillier, and S. L. Jacques. 2010. *In vivo* measurement of epidermal thickness changes associated with tumor promotion in murine models. *J. Biomed. Opt.* 15: 041514-1–041514-9.
31. Neerken, S., G. W. Lucassen, M. A. Bisschop, E. Lenderink, and T. A. Nuijs. 2004. Characterization of age-related effects in human skin: A comparative study that applies confocal laser scanning microscopy and optical coherence tomography. *J. Biomed. Opt.* 9: 274–281.
32. Papp, K. A., R. G. Langley, M. Lebwohl, G. G. Krueger, P. Szapary, N. Yeilding, C. Guzzo, M. C. Hsu, Y. Wang, S. Li, et al; PHOENIX 2 study investigators. 2008. Efficacy and safety of ustekinumab, a human interleukin-12/23 monoclonal antibody, in patients with psoriasis: 52-week results from a randomised, double-blind, placebo-controlled trial (PHOENIX 2). *Lancet* 371: 1675–1684.
33. Leonardi, C. L., A. B. Kimball, K. A. Papp, N. Yeilding, C. Guzzo, Y. Wang, S. Li, L. T. Dooley, K. B. Gordon; PHOENIX 1 study investigators. 2008. Efficacy and safety of ustekinumab, a human interleukin-12/23 monoclonal antibody, in patients with psoriasis: 76-week results from a randomised, double-blind, placebo-controlled trial (PHOENIX 1). *Lancet* 371: 1665–1674.
34. Kimball, A. B., K. B. Gordon, R. G. Langley, A. Menter, E. K. Chartash, J. Valdes; ABT-874 Psoriasis Study Investigators. 2008. Safety and efficacy of ABT-874, a fully human interleukin 12/23 monoclonal antibody, in the treatment of moderate to severe chronic plaque psoriasis: results of a randomized, placebo-controlled, phase 2 trial. *Arch. Dermatol.* 144: 200–207.
35. Griffiths, C. E., B. E. Strober, P. van de Kerkhof, V. Ho, R. Fidelus-Gort, N. Yeilding, C. Guzzo, Y. Xia, B. Zhou, S. Li, et al; ACCEPT Study Group. 2010. Comparison of ustekinumab and etanercept for moderate-to-severe psoriasis. *N. Engl. J. Med.* 362: 118–128.
36. Hueber, W., D. D. Patel, T. Dryja, A. M. Wright, I. Koroleva, G. Bruin, C. Antoni, Z. Draelos, M. H. Gold, et al 2010. Effects of AIN457, a fully human antibody to interleukin-17A, on psoriasis, rheumatoid arthritis, and uveitis. *Science Translational Med.* 2: 52ra72.